High-Sensitivity and Stable Cellular Fluorescence Imaging by Patterned Silver Nanocap Arrays

Teng Qiu,*,†,‡ Jiang Jiang,*,‡,§ Wenjun Zhang,‡ Xianzhong Lang,† Xiaoqiang Yu,† and Paul K. Chu*,‡

Department of Physics, Southeast University, Nanjing 211189, China, Department of Physics and Materials Science, City University of Hong Kong, Tat Chee Avenue, Kowloon, Hong Kong, China, and Key Laboratory of Ion Beam Bioengineering, Institute of Plasma Physics, Chinese Academy of Sciences, Hefei 230031, China

ABSTRACT Patterned silver nanocap arrays (PSNAs) prepared on porous anodic alumina templates by a simple coating technique yield enhanced sensitivity and stability in cellular fluorescence imaging. Microstructural analysis, surface-enhanced Raman scattering mapping, and finite difference time domain simulation indicate that the hot spots are evenly distributed on the substrate. Ag1522 or Chinese Hamster Ovary cells are labeled by phalloidin-fluorscein isothiocyanate (P-FITC) on the cytoskeletons and the fluorescence signals from the fluorophores bound on the cell cytoskeletons on the PSNAs are enhanced 8-fold compared to those on glass used in conventional imaging. In addition to the intensity enhancement, the photostability is improved dramatically. Spectral analysis suggests that the PSNAs can create more excitons in the light-emitting P-FITC because of plasmon resonance energy transfer from the silver nanocaps to the nearby P-FITC. They can also act as plasmonic antennae by converting a part of the nonradiative near-field emission from the fluorophores to the far field consequently enhancing the emission.

KEYWORDS: porous anodic alumina • patterned silver nanocap arrays • localized surface plasmons • cell fluorescence imaging • photostability

INTRODUCTION

Subcellular distributions of biomolecules in nuclei, plasma membranes, and cytoskeletons can be imaged and visualized by chemical reagents that bind to specific structures of the biomolecules. When the reagents have fluorescent chromophores or are coupled to fluorochromes, the cellular structures can be detected by fluorescence microscopy (1). A wide range of fluorophores with distinctive spectral characteristics are available and when bound to the targets on the cell surfaces, they show great promise in elucidating signaling pathways and performing disease diagnosis on the single molecular level (2). Various fluorescent probes such as organic dyes are commercially available to stain particular cellular structures. Although good biocompatibility and multicolor labeling are some of the advantages of these organic fluorophores, their extinction coefficients are relatively small compared to fluorescent nanoparticles, and organic fluorophores are known to emit signals with poor stability and strong blinking (3, 4). Hence, how to improve the sensitivity and photostability is a big challenge.

As a spontaneous emission process, fluorescence involves the interaction between the emitter and its environment and is therefore subject to external factors (5, 6). It is thus possible to tailor the fluorescence process to increase the emission intensity. In the first studies on fluorophore-metal interactions in the 1970s (7, 8), a fluorophore was used to interact with a smooth Ag or Au film typically about 40 nm thick. In such cases, the fluorophore creates surface plasmons which radiate at a defined angle into the substrate. Creation of surface plasmons requires illumination of a metal film through a glass prism or some higher dielectric constant materials (9, 10). The metal film must be thin so that the field penetrates from the prism side to the distal side of the metal. In general, the fluorescence intensity and lifetime are not dramatically changed. For instance, a recent report by Le Moal et al. described cell imaging on metal mirror surfaces showing that the fluorescence signals from the organic dyes on the cell surfaces were increased 4 times by the metal substrate (10). In contrast to a continuous metal surface, metal colloids interact strongly with light (11). Localized surface plasmons can be created by direct illumination of metal colloids resulting in rapid oscillation of the spatially bound electrons (12). Depending upon the distance and geometry, metal colloids can result in fluorescence enhancement by factors of up to 1000 (13, 14). The mechanism explaining the effects of metal colloids interacting with fluorophores can be understood by the formation of metal interstitial sites. These interstitial sites, so-called "hot spots" or "hot junctions" in the nanostructures, consist of two or more coupled particles or nanostructured surfaces

* Corresponding author. E-mail: tqiu@seu.edu.cn (T. Q.); jiangjiang30@gmail.com (J. J.); paul.chu@cityu.edu.hk (P. K. C.).
Received for review June 20, 2010 and accepted July 22, 2010
† Southeast University.
‡ City University of Hong Kong.
§ Chinese Academy of Sciences.
DOI: 10.1021/am100534h

with closely spaced features. They are believed to have highly concentrated electromagnetic fields associated with strong localized surface plasmon resonance (15, 16). Although spraying silver or gold colloids onto a substrate leads to a high fluorescence signal at some local hot spots, it is not easy to obtain a reliable, stable, and uniform signal spanning a wide dynamic range due to particle aggregation. Popular approaches to remedy problems such as poor control of the particle aggregation states include immobilization at surfaces (17), entrapment within stable matrices (18), or fabrication of complex surface structures (e.g., with microfabrication) (19, 20). However, these processes can be labor intensive and costly and it is sometimes impossible to extend to large dimensions. Furthermore, precise control of the gaps between the nanostructures with interparticle gap dimensions in the sub-10 nm regime necessary for intense localized surface plasmon resonance is still extremely difficult by existing nanofabrication methods (21, 22).

We recently reported a convenient nanotechnique to fabricate highly ordered hemispherical silver nanocap arrays templated by porous anodic alumina membranes suitable for robust and cost-efficient surface-enhanced Raman scattering (SERS) substrates (23). On account of the periodic hexagonal arrangement and gap control between the nanostructures in the sub-10 nm regime, a high density of hot spots can be produced to yield a large Raman signal. The surface structure can further be tuned to optimize the enhancement factor by means of porous anodic alumina fabrication and silver deposition. In this work, the fluorescence imaging capability of patterned silver nanocap arrays (PSNAs) produced by this method is studied. We first describe the physical mechanisms responsible for the efficient enhancement of the emission signals arising from the nearby fluorophores using the PSNAs as support. The organic fluorophore of phalloidin-fluorscein isothiocyanate (P-FITC) is used to label the cell cytoskeletons and cell images are monitored using confocal laser scanning microscopy. The images acquired from the PSNAs are compared to those collected on glass slides to investigate the influence of the silver nanocaps on the fluorophores localized on the cell cytoskeletons. The effects of the PSNAs on the photostability of the bound P-FITC are also demonstrated.

EXPERIMENTAL SECTION

Preparation of Patterned Silver Nanocap Arrays. Al foils (99.99% pure) 0.2 mm thick were degreased by acetone and electro-polished in a mixture of ethanol and perchloric acid with volume ratio of 5:1 under a constant direct-current voltage of 15 V for 3 min to further remove surface impurities. After being rinsed in distilled water and drying, the Al foils were anodized separately in a 0.5 M oxalic acid solution under a constant direct-current voltage of 40 V at 10 °C. To obtain an ordered nanopore array, we adopted a two-step anodizing process (24, 25). The Al foils were first anodized for 2 h followed by immersion into a mixture of chromic acid (1.8 wt %) and phosphoric acid (6 wt %) at 75 °C (1:1 in volume). After 2 h, the alumina layer that grew at the first step was removed and the surface of the foil became bright. After a second anodizing step for 2 h, the porous anodic alumina templates were obtained. Silver coatings were prepared on the porous anodic alumina templates at room temperature under argon (20 sccm) in a conventional direct-current magnetron sputtering system. A 50 mm diameter silver plate (>99.99% pure) was used as the target. The sputtering chamber was initially evacuated to a base pressure below 2.5×10^{-3} Pa and then presputtering was carried out at an argon gas pressure of 1.0 Pa for 5 min in order to clean the target surface. The power of the magnetron was ~40 W (voltage of 410 V and current of 100 mA). During deposition, the pressure in the magnetron chamber was 3.8×10^{-1} Pa and the distance between the target and substrate was 20 cm. The sputtering time was 10 min. After deposition, the samples were protected from contamination and oxidation in a vacuum desiccator until they were subjected to further experiments.

Cell Culture and Phalloidin-Fluorescein Isothiocyanate Stain. Chinese Hamster Ovary (CHO, ATCC@number: CRL-9618) cells were maintained in a complete medium made of a mixture of 45% Dulbecco's Modified Eagle Medium, 45% F-12, and 10% Fetal Calf Serum. Ag1522 cells, a normal human fibroblast culture derived from foreshins of 3-day-old male, were used at passages 10−15. The Ag1522 cells were grown in an α-minimum essential medium with 10% newborn calf serum. The cultures were maintained at 37 °C under 95% air and 5% CO_2. The subconfluent monolayers were dissociated with a 0.01% solution of trypsin and resuspendend into a fresh complete medium. Both the subconfluent monolayer CHO and AG1522 cells were washed with a phosphate buffer solution twice. Four-hundred microliters of 2% paraformaldehyde were slowly added to the phosphate buffer solution in each 60 cm Petri dish. After waiting for 20 min at 37 °C, the cultures were washed by the phosphate buffer solution three times and permeabilized with a triton buffer solution (0.1% Triton-X 100, 1% Fetal Calf Serum, in phosphate buffer solution) for 30 min at 25 °C. The P-FITC (Sigam Cat: P5282) working solution (0.1 μL/mL P-FITC in triton buffer solution) was then added. After 25 min at 25 °C, glass slides or silver coated porous anodic alumina templates were put on the monolayer of CHO and AG1522 cells. Figure S1 in the Supporting Information provides a schematic overview of the method for cell culture and P-FITC stain.

Instrumentation and Data Acquisition. Scanning electron microscopy (SEM, JEOL JSM-6335F) and atomic force microscopy (AFM, Vecco MultiMode V) were used to investigate the structures of PSNAs. The local electromagnetic fields were calculated using commercial finite difference time domain software (RSOFT FULLWAVE). The SERS mapping measurements were performed on a Horiba Jobin-Yvon LabRAM HR800 micro-Raman spectrometer with the 514 nm laser focused to a 1 μm diameter area at room temperature. The signal collection time was 1 s. For evaluation of the substrate Raman-enhancing capability, a rhodamine 6G (1×10^{-5} M) water solution was used. In order to allow molecule adsorption, the substrates were maintained for 30 min in the rhodamine 6G solution and then taken out and rinsed thoroughly. The Raman peak of rhodamine 6G at 612 cm^{-1} shown in Figure S2 in the Supporting Information was used in the SERS mapping. The UV−visible absorbance spectra were acquired on a PerkinElmer LAMBDA750 spectrophotometer. The photoluminescence (PL) spectral analysis was conducted on a Horiba Jobin-Yvon Fluorolog-3 spectrofluorometer. The cell images were captured by an inverted fluorescence microscope (Axio Observer; Carl Zeiss) and confocal laser scanning microscope (TCS SP2; Leica, Wetzlar, Germany). The relative fluorescent density was determined by Quantity One (Bio-Rad version 4.6.2) for each image.

RESULTS AND DISCUSSION

Figure 1 provides a schematic overview of the method to fabricate the PSNAs. High purity Al foils were cleaned and polished and then underwent a two-step anodizing process

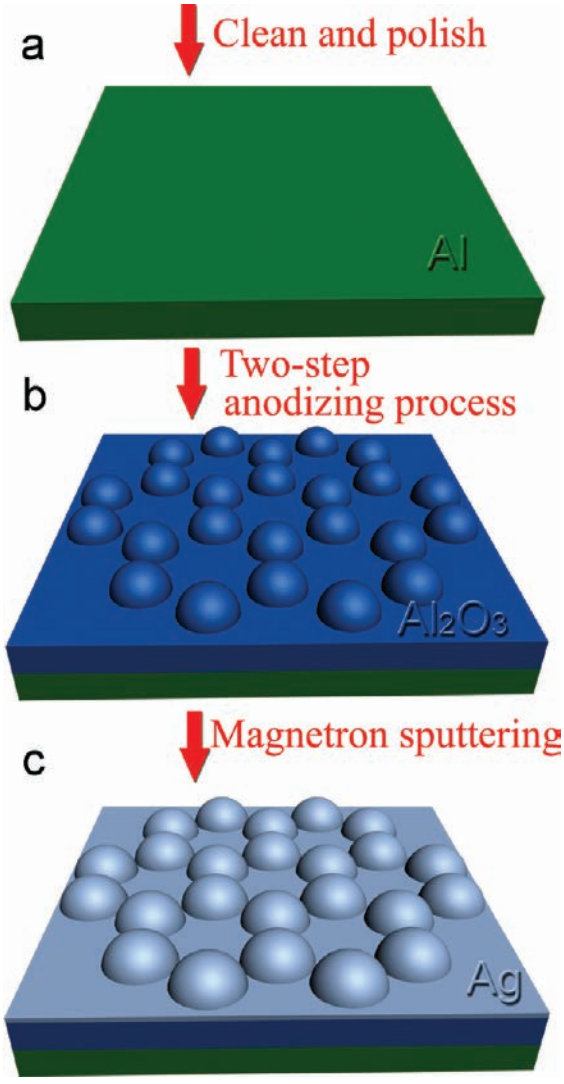

FIGURE 1. Schematic representation of the fabrication method of PSNAs.

to produce the porous anodic alumina templates (24, 25). Together with the orderly hexagonal pore array, the porous anodic alumina templates have small protrusions along the surface of the pore wall (23). During direct-current magnetron sputtering, the silver nanocaps grow on the protrusions of the porous anodic alumina templates. The use of the porous anodic alumina templates in conjunction of the versatile coating technique allows flexible and rapid production of the PSNAs. In particular, this template technique allows one to obtain size-selective, cost-effective, and controllable assemblies on a large scale.

On the basis of our previous experiments, the suitable fabrication parameters are adopted to optimize the self-organized growth of the PSNAs (23). As shown in Figure 2a, which depicts a typical SEM image of the sample surface (The inset shows large-area PSNAs with size exceeding 3 cm^2), the silver nanocaps cover the alumina protrusions and a periodic hexagonal arrangement can be observed. The structures have very uniform sizes ($D = 50 \pm 5$ nm) due to the similar shape of the alumina protrusions and same sputtering time. Ortho-, meta-, and para-cap gaps can also be observed and the ortho-cap gap (G) is less than 10 nm.

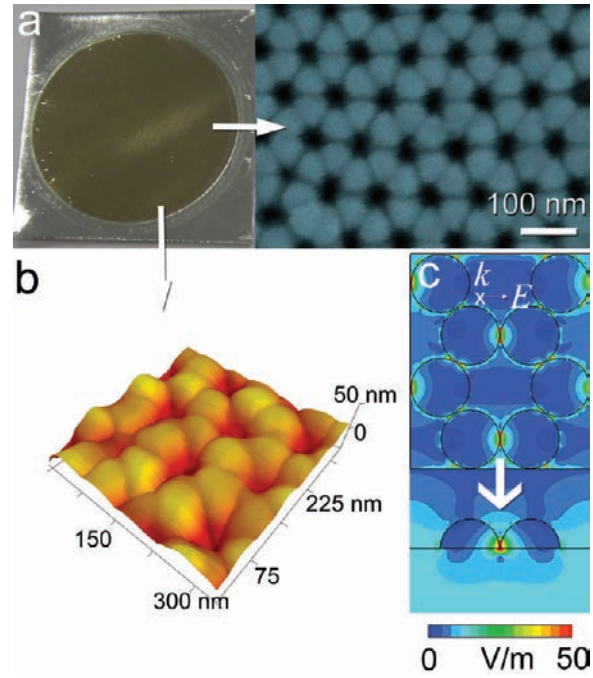

FIGURE 2. (a) SEM image and (b) 3D AFM image acquired from the PSNAs. The inset in (a) shows large-area PSNAs with the size exceeding 3 cm^2. (c) Simulated electromagnetic field distribution map of the PSNAs with parameters D = 50 nm and G = 1 nm. The inset in (c) shows the k-vector and polarization of the incident light in the simulation.

The high-resolution 3D AFM image of the same sample is displayed in Figure 2b. Protrusions can be observed along the surface of the pore wall. There is a V-shape dent between two adjacent protrusions and the hot spots are believed to be located in these V-shape ortho-cap gaps. To confirm our conjecture, the local electromagnetic fields are calculated using the finite difference time domain. The silver nanocap array is approximated by six hexagonally arranged hemispheres using dimensional parameters equal to the mean values of the samples produced experimentally. Light with a wavelength of 500 nm irradiates the sample in the normal direction. Figure 2c shows the planar and cross-sectional contour plots of the near electromagnetic field distribution. The maximum local electric field in the V-shaped ortho-cap gap is calculated to be 288.6 V/m.

The homogeneity of the PSNAs is evaluated by 2D point-by-point SERS mapping of rhodamine 6G molecules as shown in Figure 3. The silver coated porous anodic alumina template is dipped in a 1×10^{-5} M rhodamine 6G water solution for 30 min and then rinsed with water. The mapping area is $20.0 \times 20.0\ \mu m^2$ and the scanning step is 1 μm. The relative SERS peak intensity of the collection spots is centered within a narrow range, and the spot-to-spot relative standard deviation is calculated to be 5%. This indicates that the substrate homogeneity is quite good and strict control of the preparation conditions can ensure good reproducibility among different batches.

We next study the PL properties of the P-FITC coupled PSNAs. P-FITC, a derivative of fluorescein used in many applications including cell labeling, has excitation and emission wavelengths of approximately 495 nm/520 nm (1). The

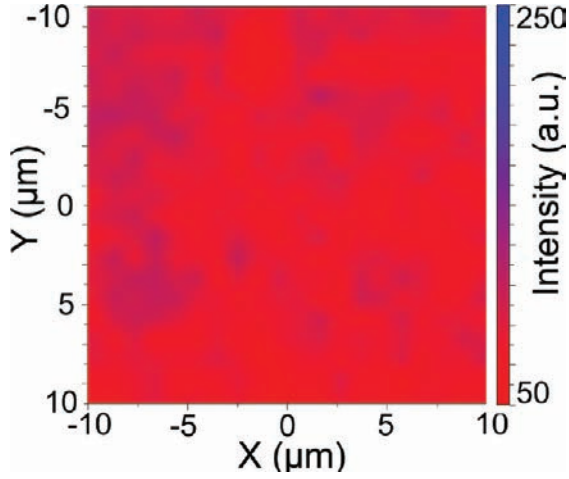

FIGURE 3. SERS map of a 20.0 × 20.0 μm^2 area of the PSNAs. The map is obtained from the integrated intensity of the 612 ± 10 cm^{-1} band of 1 × 10^{-5} M rhodamine 6G adsorbed on the substrate. Each point in the map was taken using 20 mW 514 nm excitation with a 1 s integration time.

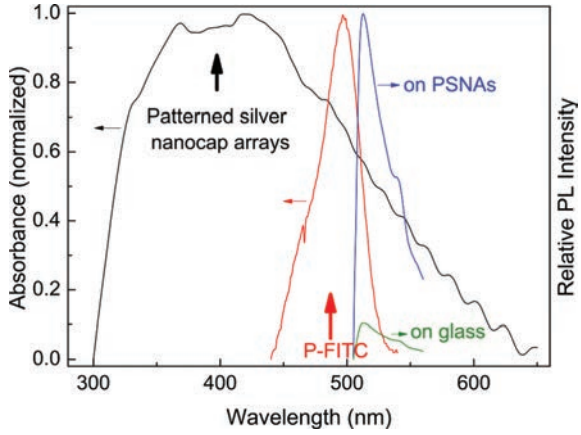

FIGURE 4. Optical absorption spectra of PSNAs and P-FITC compared to the PL spectra of P-FITC coupled PSNAs and P-FITC coupled glass.

P-FITC working solution (0.1 μL/mL P-FITC in triton buffer solution) was coupled to PSNAs and glass by means of the drop coating of the solution onto the sample. The PL spectra of P-FITC coupled PSNAs and P-FITC coupled glass excited by the 495 nm line of a Xe lamp for the same time of 0.1 s are compared in Figure 4 (right). The peak intensity of the PL spectrum of the P-FITC coupled PSNAs is about 9 times higher than that of the P-FITC on glass. The enhancement of the PL efficiency may originate from the plasmon resonance energy transfer from silver nanocaps to the nearby P-FITC. This is confirmed by the optical absorption spectra in Figure 4 (left). The peaks at 495 nm from the P-FITC and UV−vis absorption from 300 to 600 nm from the PSNAs representing the localized surface plasmon energy, respectively, are observed. It should be noted that the large UV−vis absorption band of the PSNAs is caused by the gaps with various sizes between neighboring silver nanocaps (ortho-, meta-, and para-cap gaps) on the samples (15, 26). Similar to the donor−acceptor energy matching in fluorescent (or Förster) resonance energy transfer between two fluorophores, critical matching between the localized surface plasmon resonating energy E_p (2.07−4.13 eV, equivalent to 300−600 nm) in the PSNAs and the electron transition energy from ground to excited state $E_e - E_g$ (2.51 eV, equivalent to 495 nm) in the P-FITC permits the plasmon resonance energy transfer process. The quantized energy is likely transferred through the dipole−dipole interaction between the resonating plasmon dipole in the nanocaps and P-FITC dipole. In previous work on the surface plasmon-mediated fluorescent resonance energy transfer process (27), the surface plasmon resonance shift due to redox molecules (28) and bulk optical extinction spectroscopy of nanoplasmonic particle clusters with conjugated resonant molecules (29) also suggest the possibility of such dipole−dipole interactions. Consequently, the resulting resonance (localized surface plasmon resonance coupling due to the hybrid junction of P-FITC and sliver nanocaps) can spur energy transfer from the sliver nanocaps to the light-emitting P-FITC under irradiation by the 495 nm Xe line. This process creates more excitons in the light-emitting P-FITC.

Besides enhancing excitation of nearby fluorophores, the PSNAs may affect the emission from the P-FITC. Recent studies have unveiled an enhancement mechanism based on strong coupling between the excited state of the emitter and plasmons (30−32). A fluorophore in the excited state can interact with a nearby metal nanoparticle to create plasmons. Here, the metal nanoparticles act as plasmonic antennae by converting a part of the fluorophore's nonradiative near-field emission into far-field emission thereby creating the observed emission. The emission retains the same spectrum of the fluorophore. To optimize the efficiency of this process, a good spectral overlap between the emission band and localized surface plasmon resonance band of the metallic substrate is needed (33, 34). By analyzing Figure 4, one can notice that the enhancement is further optimized in terms of spectral overlap between the localized surface plasmon band of the PSNAs and emission band of the P-FITC.

It should be noted that the silver coated porous anodic alumina templates are protected from contamination or oxidation in a vacuum desiccator until further experiments. This special precaution minimizes oxidation of Ag so that silver instead of silver oxide contributes to the cellular fluorescence images acquired by confocal laser scanning microscopy. Figure 5 exhibits the fluorescence images of the P-FITC-labeled AG1522 cell samples on the PSNAs compared to those on glass. It can be observed that the intensity of the fluorophores on the PSNAs is much higher (Figure 5b) and the intensity ratio of the emission spots to background increases by a factor of 8. It is known that fluorescence is enhanced only when the fluorophore is localized at an optimal distance close to the surface of the metal nanoparticle in the range of 5−30 nm (35, 36). In this case, because the membranes of the cells are about 7 nm thick (37), some fluorophores on the cell cytoskeletons that adhere to the metal substrate may be localized within this enhancement region. Hence, it can be inferred that enhancement of the

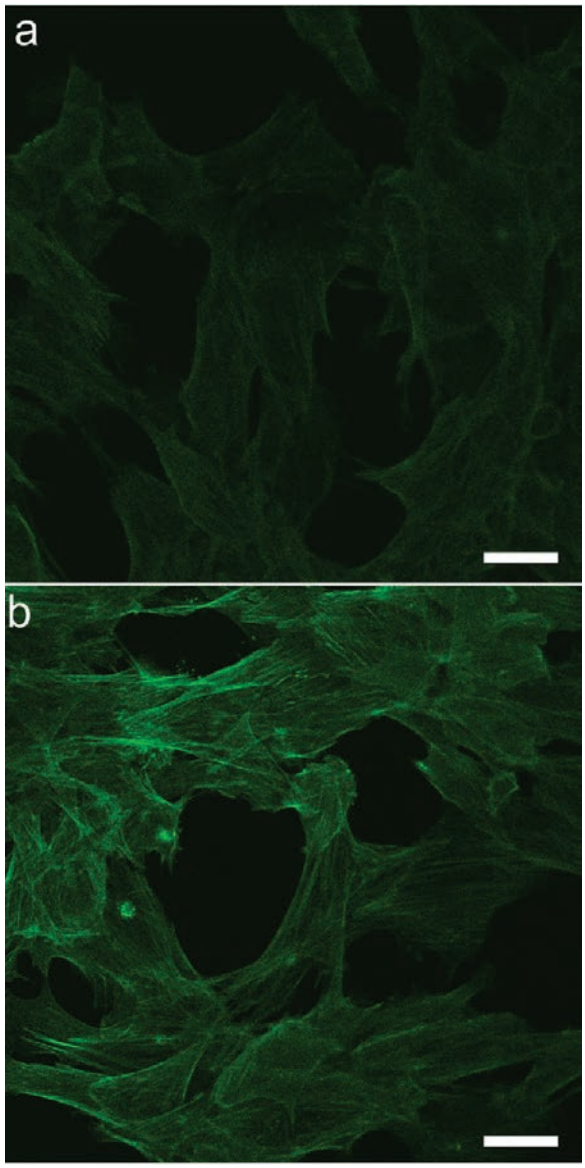

FIGURE 5. Representative confocal images of AG1522 cells labeled with P-FITC adhered to the cytoskeleton protein f-actin on the (a) glass slide and (b) PSNAs excited by the 488 nm laser line. Both images are in pseudo color and the scale bar is 20 μm.

emission signals from the cell cytoskeletons observed in this study is due to the coupling effect between the P-FITC and PSNAs.

The photostability of P-FITC-labeled CHO cells on the PSNAs is compared to that of labeled cells on glass. Figure 6 depicts the quantitative changes in the fluorescence intensity observed from the P-FITC labeled CHO cells on the PSNAs and glass (also see fluorescence images in Figures S3 and S4). The intensity of excitation were the same for labeled cells on glass and PSNAs. Fluorescence from the P-FITC labeled CHO cells on glass is quenched in 2 min. In contrast, fluorescence from the P-FITC-labeled CHO cells on the PSNAs diminishes to half of its original intensity in 3 min, after which fluorescence is maintained for more than 12 min. The results suggest that the fluorophores near the glass are destroyed, whereas those near the PSNAs are more photostable.

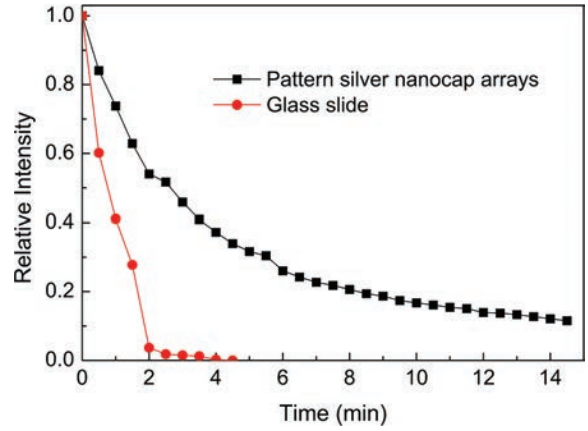

FIGURE 6. Photostability tests on P-FITC labeled CHO cells on the PSNAs and glass slide. The excitation source is a mercury lamp operated at 450 to 490 nm.

CONCLUSION

In summary, PSNAs prepared by a simple coating technique using porous anodic alumina templates are demonstrated to be excellent substrates for cellular fluorescence imaging. The fluorescence signals from the fluorophores bound on the cell cytoskeletons are enhanced significantly by the PSNAs compared to glass used in conventional experiments. In addition to the enhanced intensity, the photostability is dramatically improved. On account of the large UV−vis absorption band of the PSNAs, most fluorescent probes with visible light emission may exhibit improved sensitivity and photostability when coupled onto the substrate. Since low cytotoxicity is expected on silver films (38), the use of PSNAs is a good means to improve the sensitivity and stability of cellular fluorescence imaging. The method is expected to unveil more subtle details from living cells and tissues without needing to resort to a more intense excitation source that may otherwise damage the biological media.

Acknowledgment. T. Q. and J. J. contributed equally to this work. This work was supported jointly by the National Natural Science Foundation of China under Grant 50801013 and 10947129, Natural Science Foundation of Jiangsu Province, China under Grant No. BK2009291, Specialized Research Fund for the Doctoral Program of Higher Education under Grant 200802861065, the Excellent Young Teachers Program of Southeast University, and the Hong Kong Research Grants Council (RGC) General Research Fund (GRF) CityU 112307.

Supporting Information Available: A schematic overview of the method for cell culture and P-FITC stain, typical SERS spectra obtained from 1×10^{-5} M R6G adsorbed on PSNAs and P-FITC-labeled CHO cell images acquired on the PSNAs and glass slides demonstrating photostability (PDF). This material is available free of charge via the Internet at http://pubs.acs.org.

REFERENCES AND NOTES

(1) Suzuki, T.; Matsuzaki, T.; Hagiwara, H.; Aoki, T.; Takata, K. *Acta Histochem. Cytochem.* **2007**, *40*, 131–137.
(2) Chen, I.; Ting, A. Y. *Curr. Opin. Biotechnol.* **2005**, *16*, 35–40.
(3) Fan, J. Y.; Li, H. X.; Jiang, J.; So, L. K. Y.; Lam, Y. W.; Chu, P. K. *Small* **2008**, *4*, 1058–1062.

(4) Rosenthal, S. J.; Tomlinson, A.; Adkins, E. M.; Schroeter, S.; Adams, S.; Swafford, L.; McBride, J.; Wang, Y. Q.; DeFelice, L. J.; Blakely, R. D. *J. Am. Chem. Soc.* **2002**, *124*, 4586–4594.
(5) Barnes, W. L. *J. Mod. Opt.* **1998**, *45*, 661–699.
(6) Lakowicz, J. R. *Anal. Biochem.* **2001**, *298*, 1–24.
(7) Drexhage, K. H. *J. Lumin.* **1970**, *1*, 693–701.
(8) Persson, B. N. J. *J. Phys. C: Solid State Phys.* **1978**, *11*, 4251–4269.
(9) Choumane, H.; Ha, N.; Nelep, C.; Chardon, A.; Reymond, G. O.; Goutel, C.; Cerovic, G.; Vallet, F.; Weisbuch, C.; Benisty, H. *Appl. Phys. Lett.* **2005**, *87*, 031102.
(10) Le Moal, E.; Fort, E.; Lévêque-Fort, S.; Cordelières, F. P.; Fontaine-Aupart, M. P.; Ricolleau, C. *Biophys. J.* **2007**, *92*, 2150–2161.
(11) Kelly, K. L.; Coronado, E.; Zhao, L. L.; Schatz, G. C. *J. Phys. Chem. B* **2003**, *107*, 668–677.
(12) Link, S.; El-Sayed, M. A. *Int. Rev. Phys. Chem.* **2000**, *19*, 409–453.
(13) Chumanov, G.; Sokolov, K.; Gregory, B. W.; Cotton, T. M. *J. Phys. Chem.* **1995**, *99*, 9466–9471.
(14) Sokolov, K.; Chumanov, G.; Cotton, T. M. *Anal. Chem.* **1998**, *70*, 3898–3905.
(15) Hutter, E.; Fendler, J. H. *Adv. Mater.* **2004**, *16*, 1685–1706.
(16) Qiu, T.; Wu, X. L.; Shen, J. C.; Chu, P. K. *Appl. Phys. Lett.* **2006**, *89*, 131914.
(17) Kubo, S.; Gu, Z. Z.; Tryk, D. A.; Ohko, Y.; Sato, O.; Fujishima, A. *Langmuir* **2002**, *18*, 5043–5046.
(18) Kuncicky, D. M.; Prevo, B. G.; Velev, O. D. *J. Mater. Chem.* **2006**, *16*, 1207–1211.
(19) Yu, F.; Tian, S. J.; Yao, D. F.; Knoll, W. *Anal. Chem.* **2004**, *76*, 3530–3535.
(20) Ebbesen, T. W.; Lezec, H. J.; Ghaemi, H. F.; Thio, T.; Wolf, P. A. *Nature* **1998**, *391*, 667–669.
(21) Jiang, J.; Bosnick, K.; Maillard, M.; Brus, L. *J. Phys. Chem. B* **2003**, *107*, 9964–9972.
(22) Wang, H. H.; Liu, C. Y.; Wu, S. B.; Liu, N. W.; Peng, C. Y.; Chan, T. H.; Hsu, C. F.; Wang, J. K.; Wang, Y. L. *Adv. Mater.* **2006**, *18*, 491–495.
(23) Qiu, T.; Zhang, W. J.; Lang, X. Z.; Zhou, Y. J.; Cui, T. J.; Chu, P. K. *Small* **2009**, *5*, 2333–2337.
(24) O'Sullivan, J. P.; Wood, G. C. *Proc. R. Soc. London, Ser. A* **1970**, *317*, 511–543.
(25) Shingubara, S.; Okino, O.; Sayama, Y.; Sakaue, H.; Takahagi, T. *Jpn. J. Appl. Phys., Part 1* **1997**, *36*, 7791–7795.
(26) Ghosh, S. K.; Pal, T. *Chem. Rev.* **2007**, *107*, 4797–4862.
(27) Andrew, P.; Barnes, W. L. *Science* **2004**, *306*, 1002–1005.
(28) Boussaad, S.; Pean, J.; Tao, N. *J. Anal. Chem.* **2000**, *72*, 222–226.
(29) Haes, A. J.; Zou, S. L.; Zhao, J.; Schatz, G. C.; Van Duyne, R. P. *J. Am. Chem. Soc.* **2006**, *128*, 10905–10914.
(30) Chowdhury, M. H.; Gray, S. K.; Pond, J.; Geddes, C. D.; Aslan, K.; Lakowicz, J. R. *J. Opt. Soc. Am., B* **2007**, *24*, 2259–2267.
(31) Zhang, J.; Fu, Y.; Liang, D.; Nowaczyk, K.; Zhao, R. Y.; Lakowicz, J. R. *Nano Lett.* **2008**, *8*, 1179–1186.
(32) Colas des Francs, G.; Bouhelier, A.; Finot, E.; Weeber, J. C.; Dereux, A.; Girard, C.; Dujardin, E. *Opt. Express* **2008**, *16*, 17654–17666.
(33) Gerber, S.; Reil, F.; Hohenester, U.; Schlagenhaufen, T.; Krenn, J. R.; Leitner, A. *Phys. Rev. B* **2007**, *75*, 073404.
(34) Farcău, C.; Aştilean, S. *Appl. Phys. Lett.* **2009**, *95*, 193110.
(35) Zhang, J.; Malicka, J.; Gryczynski, I.; Leonenko, Z.; Lakowicz, J. R. *J. Phys. Chem. B* **2005**, *109*, 7969–7975.
(36) Mertens, H.; Koenderink, A. F.; Polman, A. *Phys. Rev. B* **2007**, *76*, 115123.
(37) Alberts, B.; Johnson, A.; Lewis, J.; Raff, M.; Roberts, K.; Walter, P. *Molecular Biology of the Cell*, 5th ed.; Garland Science: New York, 2007.
(38) Zhang, J.; Fu, Y.; Liang, D.; Zhao, R. Y.; Lakowicz, J. R. *Langmuir* **2008**, *24*, 12452–12457.

AM100534H